ChemElectroChem

Articles
doi.org/10.1002/celc.202101135

Chemistry Europe
European Chemical Societies Publishing

www.chemelectrochem.org

Gas flow Stimulated Hydrodynamics for Preparation and Application of Platinized Titanium Hollow Fibre Electrodes

Ronald P. H. Jong and Guido Mul*[a]

In this study, Pt was electrodeposited on the surface of Ti hollow fibres from $PtCl_6^{2-}$ solution at fixed potential and at variable gas flow rate. Partial Pt coverage of Ti was obtained at flow rates ≤ 5 mL·min^{-1}, while a more-even geometrical distribution and linearly increasing Electrochemical Surface Area (ECSA) of Pt was obtained for flow rates of >5 and <20 mL·min^{-1}. Above 20 mL·min^{-1}, the morphology did not significantly change, and only a limited increase in ECSA of Pt (Pt_{ECSA}) was observed. Second, the performance of the Pt functionalized Ti-HFEs was evaluated at fixed potential in i) liquid phase oxidation of Fe^{II} to Fe^{III}, and ii) the hydrogen (gas) evolution reaction (HER). Generally, for the oxidation of Fe(CN)$_6^{4-}$, a linear increase in current from 3 to ≈ 9 mA was found as a function of increasing gas flow rate. For the HER, a gas evolving reaction, initially (in the range of 0–10 mL·min^{-1}) a much larger enhancement in current (from $\approx$-10 to -35 mA) was observed than consecutively at higher flow rates. The effect of gas flow rate on Pt deposition, and utilization of platinized Ti HFEs, is explained on the basis of increasing fractional participation of relatively small pores at high flow rates, and generally an increasing mass transfer coefficient (k_M) associated with localized mixing of the electrolyte near the electrode/electrolyte interface. The k_M is roughly in the same order of magnitude as obtained in experiments using rotating disc electrodes.

Introduction

Hollow fibre electrodes (HFEs) made from sintered metallic particles receive considerable attention in the electrochemistry community, since they i) are easily prepared, ii) offer high stability and large surface area, and iii) can be made from various metals.[1–5] HFEs have been mainly prepared from Cu and utilized in the electrochemical reduction of CO$_2$.[3,6–9] While these electrodes perform remarkably well when gas is exiting through the porous wall, the origin of the improved performance by gas flow is only generally attributed to enhanced mass transfer, without further quantification.

We have recently shown how porous Ti based hollow fibres with low electrical resistivity (4.1–9.6 μΩ m) can be produced by dry-wet spinning and carefully designed thermal treatment steps.[5] One of the developed thermal treatment steps results in porous metallic Ti based fibres, which are very suitable for electrochemical applications, in particular after functionalization with electrocatalytically active metals. Electrodeposition has been used to functionalize Cu HFEs with e.g. Au or Ni[6] and Bi-based nanosheets.[9] Yet the effect of preparation conditions (applying gas flow) on the obtained metal distribution has not

been extensively investigated. In the present study we first discuss the effect of gas flow rate on electrodeposition of Pt on Ti-HFEs. Microscopy was used to visually locate the active Pt particles on the HFE, and electrochemical methods were employed to identify the activity of the deposit under several flow conditions. In the present study we demonstrate that the gas flow rate can be used to alter the coverage of the Ti particles by Pt. By studying liquid phase oxidation of Fe^{II} to Fe^{III}, and the hydrogen evolution reaction at various gas flow rates, the enhancement in mass transfer coefficient by exiting gas flow is further described and discussed.

Results and Discussion

Platinum electrodeposition at variable inert gas velocity

The Ti hollow fibres were prepared and characterized as described in previous work.[5] For the electrodeposition of Pt on a Ti-HFE, $PtCl_6^{2-}$ was dissolved at fixed concentration, and deposition [Eq. (1)] was performed using a fixed potential and deposition time, varying the inert gas flow (Flow$_{Pt\text{-}dep}$) from 5 to 40 mL·min^{-1}. The surface coverage, quantified by the Pt_{ECSA} normalized to the geometric area, is shown in Figure 1 as a function of gas flow rate. It should be mentioned that at the potential used for electrodeposition, the HER [Eq. (2)] takes place once some initial amount Pt has been deposited. Additionally, Cl$_2$ [Eq. (3)] and O$_2$ [Eq. (4)] are produced at the counter electrode during electrodeposition, which can also be reduced at the HFE cathode. Therefore, the quantity of deposited Pt cannot be directly correlated to the charge passed through the cell.

[a] R. P. H. Jong, Prof. Dr. G. Mul
Photocatalytic Synthesis Group
University of Twente
PO Box 217, 7500 AE
Enschede, The Netherlands
E-mail: g.mul@utwente.nl

ChemElectroChem

Articles
doi.org/10.1002/celc.202101135

**Chemistry
Europe**
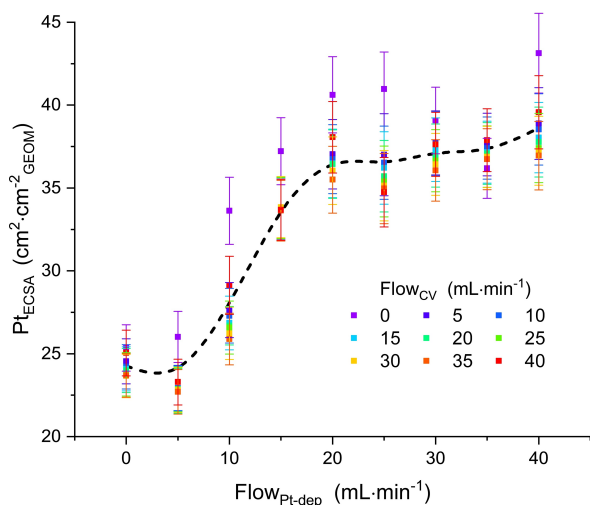European Chemical
Societies Publishing

Figure 1. Platinum electrochemical active surface area (ESCA) as a function of Ar flow applied during electrodeposition. The ECSA of platinum was determined from the adsorbed hydrogen oxidation charge, in 0.1 M HClO$_4$, applying several Ar flow rates (see colour code for Flow$_{CV}$ ranging from 0 to 40 mL·min^{-1}), providing several data points for each flow condition during Pt electrodeposition (Flow$_{Pt-dep}$). The values are normalized to the geometrical surface area of the exposed hollow fibre electrode.

$$Pt^{4+} + 4e^- \rightarrow Pt \tag{1}$$

$$2H^+ + 2e^- \rightarrow H_2 \tag{2}$$

$$2\,Cl^- \rightarrow Cl_2 + 2e^- \tag{3}$$

$$2H_2O \rightarrow O_2 + 4H^+ + 4e^- \tag{4}$$

Three distinct regions in the obtained correlation between flow rate and normalized Pt$_{ECSA}$ can be observed, first from 0 to 5 mL·min^{-1}, leading to ≈25 cm^2·cm^{-2}$_{GEOM}$, second from 5 to 20 mL·min^{-1}, following a mostly linear increase from ≈25 cm^2·cm^{-2}$_{GEOM}$ to ≈35 cm^2·cm^{-2}$_{GEOM}$, and third from 20 to 40 mL·min^{-1}, leading to a rather flow independent normalized Pt area similar to 35 cm^2·cm^{-2}$_{GEOM}$. Multiple datapoints are shown for each gas flow rate applied during Pt deposition (Flow$_{Pt-dep}$), which were obtained by varying the flow rate (Flow$_{CV}$) during the determination of the charge required for

oxidation of Pt-H$_{ads}$ (see Supplementary Information, Figure S2, for the electrochemical data). In the absence of flow during the oxidation of Pt-H$_{ads}$, the values determined for the Pt$_{ECSA}$ are typically larger by ≈5 cm^2·cm^{-2}$_{GEOM}$ when compared to those determined in Flow$_{CV}$ conditions, and a minor decrease in Pt$_{ECSA}$ is observed as a function of increasing Flow$_{CV}$ (5 to 40 mL·min^{-1}).

XPS Analysis of the obtained platinized HFEs shows that Pt is deposited in the metallic (Pt(0)) state (Figure S3), in the presence of some residual Cl$^-$ (Figure S4). Oxidation of the Ti surface of the hollow fibre was evident by comparison of the Ti 2p (Figure S5) and the O 1s spectra (Figure S6) with references. Finally some surface carbonate is likely present, as evident from the C 1s spectrum (Figure S7).

Representative SEM images of the platinized Ti-HFEs are presented in Figures 2A and 2B, revealing two types of deposition. The scattered and partial coverage of Pt on Ti as shown in image A is obtained by electrodeposition in the absence of gas flow. Image B shows the Pt coverage when 30 mL·min^{-1} was used. Generally, Pt is deposited on the outer wall of the hollow fibre, while a limited amount of small Pt particles deposits in the interior of the pore structure up to ≈12 μm inward, as can be deduced from the image shown in Figure 2C. Such distribution is likely the result of the limited depth of penetration (≈12 μm) of the PtCl$_6$$^{2-}$ solution into the pore structure, a depth similar to the dimensions of the two outer-most Ti particles. Cross sectional and surface images where taken for all of the samples and are available in the supporting information, Figures S8 to S25. For the samples from 5 to 20 mL·min^{-1} different surface regions could be distinguished, showing one or the other type of surface coverage (Figure 2A or Figure 2B). We will now discuss why an apparent bimodal distribution is obtained at low flow rates, gradually transforming to a homogeneous deposition alike the image shown in Figure 2B.

The participation of pore sizes in exiting gas

Using capillary flow porometry, the pore size distribution of the Ti hollow fibre was determined. Please see the supplementary
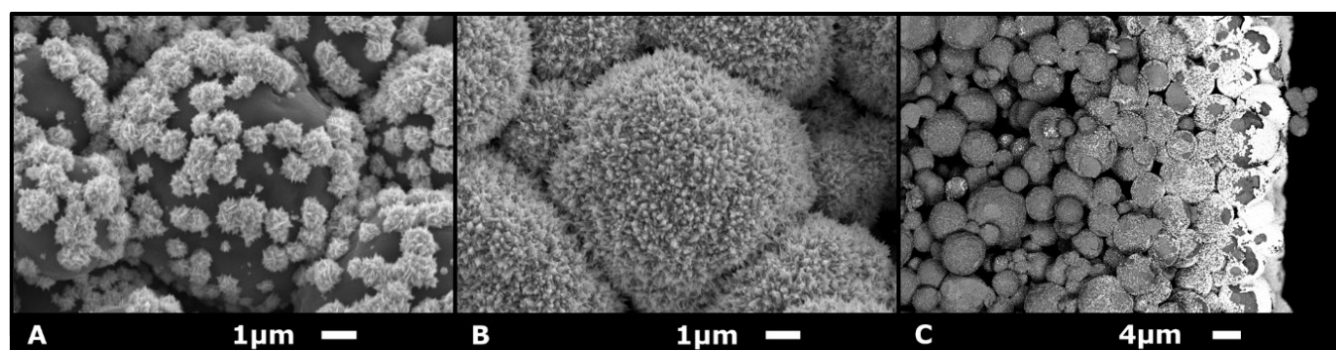

Figure 2. Platinum coverage of the titanium hollow fibre electrode. A) SEM image of deposit obtained without gas flow through the electrode wall. B) SEM image of deposit obtained when 30 mL·min^{-1} gas flow was applied through the electrode wall. C) HR-SEM ESB image of the cross section of the Pt/Ti HFE obtained using 30 mL·min^{-1} of flow through the electrode wall.

information for further details. This distribution was used to construct Figure 3, which demonstrates which fraction of the pore dimensions participates in the exiting flow at various gas flow rates. These values (indicated by the colour code) were determined by measurement of the pressure required in the interior of the fibre to obtain a certain exiting gas flow, and using the Young-Laplace Equation (5), in which ΔP is the Laplace pressure, γ the surface tension, θ the contact angle and d the pore diameter.[10–12]

$$\Delta P = \frac{4\,\gamma\,\cos(\theta)}{d} \tag{5}$$

The values applied in Equation (5) hold for aqueous electrolyte[13] and titanium oxide (the presumed surface composition on the basis of the XPS data).[12] Please see the supporting information, including Figures S26–S30) for more detail on how the Laplace equation was applied, and which assumptions and data representations were used. Within Figure 3 two representations of the fraction of pores participating in exiting flow are provided, i.e. as a value in percentage (left axis) of the total flow corresponding to a certain pore diameter, and the cumulative contribution (right axis) from large (3.0 μm), to small pores (≈ 1.25 μm). Figure 3 shows that the dominantly present pore sizes are in the range of 1.5 to ≈ 1.7 μm).

Since the pores are randomly distributed across the entire HFE, the degree of pore size participation within the PSD is to be considered randomized in location too (A simplified planer representation of the PSD utilization, in terms of open and closed pores, is provided in the supporting information, Figures S31–S40). This consideration explains the randomized distribution of the two identified types of deposit in the SEM images (see supporting information Figures S8–S25).
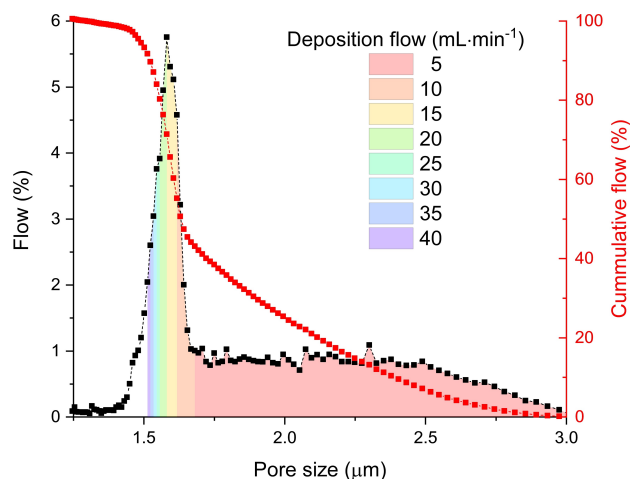
Explaining the Pt distribution and trend in Pt$_{ECSA}$

While qualitatively the Pt distribution observed in the SEM images can be understood on the basis of Figure 3, we will now discuss the flow rate dependent trend shown in Figure 1 for the obtained Pt$_{ECSA}$, with the aid of Figure 4. Figure 4 shows a schematic representation of gas-liquid distributions present in various stages of stagnant, or exiting gas for a certain pore size. The pore size is determined by the distance between two Ti-particles. Stage A shows most of the surface of the Ti particles is in contact with liquid. This is likely the situation representing i) no exiting flow at all, or ii) the smaller pores at low gas velocities (when these do not participate in the exiting flow). Stages B to D show the transient in gas-liquid-solid contact occurring during the exiting of a bubble, implying that the average time-dependent extent of contact between the electrolyte and the particle is significantly smaller than in situation A. In stage D the velocity of the bubble induces liquid convection, enhancing mass transfer of dissolved species towards the surface of the electrode.[14,15]

Situation A leads to the scattered distribution of the Pt particles on a single Ti particle, observed in Figure 2A, and the accompanying relatively low Pt$_{ECSA}$. Nucleation of Pt in this situation apparently occurs on preferred locations of the Ti particle(s). During electrodeposition the electrolyte close to the
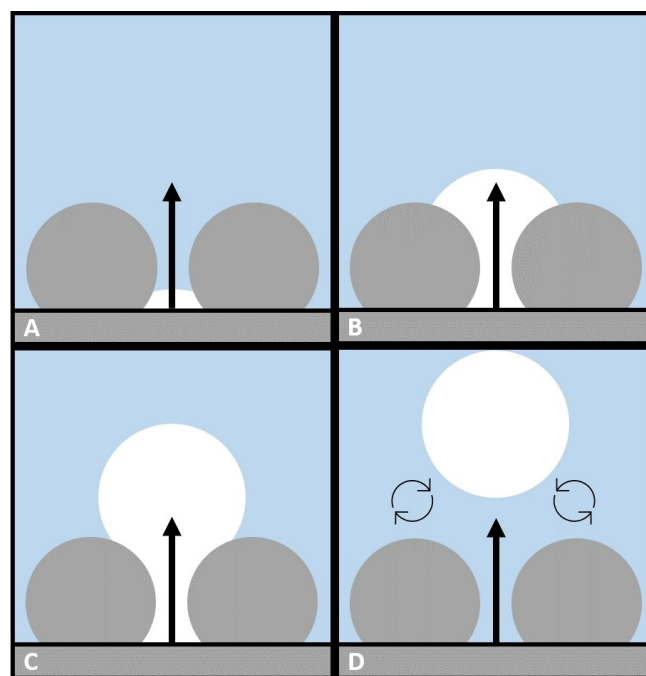

Figure 4. Schematic representation of the changing electrode-electrolyte contact area induced by gas bubbles forming in, and exiting from a pore of the HFE. The grey circles represent the Ti particles at the HFE surface, the blue surrounding is the electrolyte and the white area represents the gas phase. The black arrow indicates the direction of gas flow out of the pore. A) Initially the electrolyte occupies the pore. B) The electrolyte is displaced by the gas phase, when the pressure on the inside of the HFE is sufficiently large. C) A gas bubble occupies a significant part of the surface of the HFE. D) Desorption of the bubble results in convective mixing and re-establishment of the liquid-solid interface. The circular arrows represent this convective mixing induced by release of the gas bubble.

Figure 3. Pore size distribution of the Ti-HFE used in this work and the estimated degree (Flow %, left axis) to which each pore contributes to the exiting flow when applied in electrochemistry (see colour code). The red curve shows the cumulative of these percentages (right axis). Per example, the graph shows that at 5 mL·min⁻¹ (see red colour code) pores in the range of 1.65 to 3.0 μm participate in the exiting flow. The smaller pores, constituting the largest fraction of the total in a narrow size window, start to participate at higher flow rates, demonstrating a steep cumulatively rising contribution (in flow %) in the flow range of 10 to 25 mL·min⁻¹.

electrode is depleted of Pt ions, resulting in concentration polarization.[16] In other words, deposition is limited by transport of the $PtCl_6^{2-}$ ions by diffusion through the stagnant liquid boundary layer towards the surface. When gas is effectively exiting a pore (the case at low gas velocities only for the larger pore sizes, and at e.g. 30 mL for most of the pores), a more homogeneous coverage of Pt is obtained (in agreement with the observed larger Pt_{ESCA}). This is the result of the effective transport of the $PtCl_6^{2-}$ ions towards the surface by convection, overcompensating the lower, time averaged, extent of contact between the liquid and the solid in these conditions.

Furthermore, the phenomena shown in Figure 3 B–D likely reduce the thickness of the boundary-layer (also referred to as the Nernst diffusion layer). While less influential on the overall Pt coverage across the HFE (likely due to deposition of Pt on already present Pt particles/structures), an increasing flux at the highest gas flow rates does explain the slightly increasing trend in the Pt_{ECSA} above 20 mL·min^{-1} (Figure 1) which can be interpreted as increased surface roughness (SEM images in the supporting information, Figure S8–S25).

In summary, the Pt_{ECSA} of the Pt@Ti-HFE depends on localized mixing near a pore. The degree of localized mixing will depend on the collection of pores within the PSD that participate in the exiting flow. Within the given PSD and experimental system this entails that the most abundant pore sizes are coming 'on-line' between 5 and 20 mL·min^{-1}. Consequently, a notable enhancement in the total Pt coverage of the Ti-HFE and consequent Pt_{ECSA}, is found within this range of flow rates. Secondary effects of the enhanced flowrate are the linear velocity per pore, or rather bubble frequency, which enhances mixing and removal of H_2 gas from the surface, as will be discussed in one of the following paragraphs.

The case of oxidation of Fe^{II} to Fe^{III}

Platinized Ti hollow fibre electrodes (Pt@Ti-HFEs) prepared at gas velocity of 20 mL·min^{-1} were applied in the oxidation of a solution containing $Fe(CN)_6^{4-}$.

Figure 5 shows the I–V curves of the oxidation of Fe^{II} to Fe^{III}, Equation (6), at several gas flow rates. The outer-sphere electron transfer from $[Fe(CN)_6]^{4-}$ to the electrode is the only reaction step and occurs without binding or adsorbing either the reactant, product or intermediate on the electrode.[16–18]

$$[Fe(CN)_6]^{4-} \rightarrow [Fe(CN)_6]^{3-} + e^- \qquad (6)$$

A clear effect of flow is readily observed in Figure 5A, showing an increasingly larger limiting current as a function of increasing gas velocity. In Figure 5B the current found at 1.2 V vs RHE is plotted as a function of gas velocity. Initially, from 0 to 5 mL·min^{-1}, the effect of flow on increasing the current is the largest, which can be explained by considering that any gas purge will induce convection near the HFE. As previously explained for the curve associated with the deposition of Pt (Figure 1), the degree of effective mixing is determined by two factors; i) the participation of a certain fraction of the pore sizes
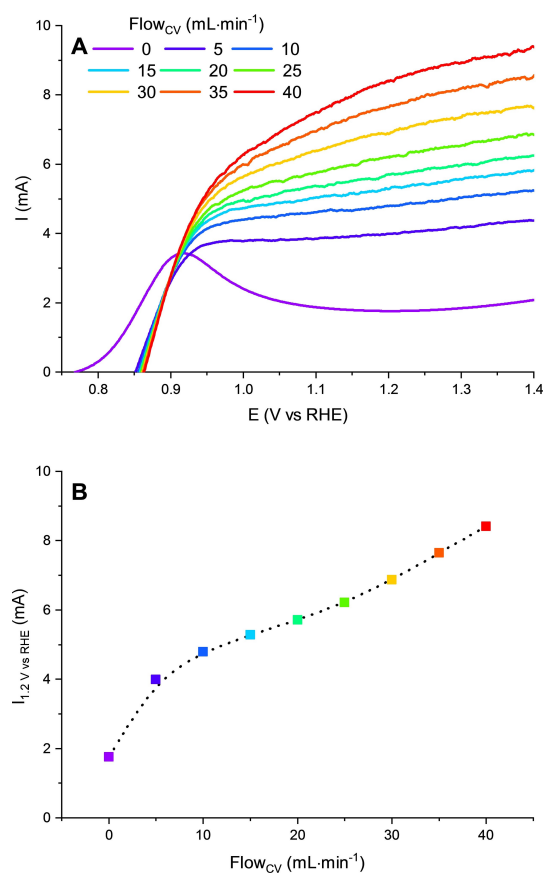
present near the surface of the fibre, and ii) the flux through a pore. Increasing the flow rate in the range from 5 to around 20 or 25 mL·min^{-1} allows participation in exiting gas of not only the larger, but also the predominantly present smaller pores. Contrary to the obtained Pt_{ESCA}, above 25 mL·min^{-1} to at least 40 mL·min^{-1} the current linearly increases. It would therefore seem these gas fluxes still enhance the mass transfer by intensified mixing of the electrolyte, which is relevant for the kinetically favourable Fe(II) oxidation reaction as is summarized in Figure 6. The increasing gas flux, above values when the degree of pore participation approximates unity, likely affects the value of the so-called Nernst diffusion layer, for example used to describe the hydrodynamics involved in rotating disc electrodes (RDEs).[16,17,19]

The case of hydrogen evolution

The hydrogen evolution reaction (HER) in acidic media (2) is a two electron transfer reaction that starts when a proton is reduced and adsorbed on the electrode surface [Eq. (7)]. This initial step can be followed by one of the following two steps. Either H_2 is formed and desorbed through a recombination step (Tafel) of two adsorbed protons [Eq. (8)], or an electrochemical
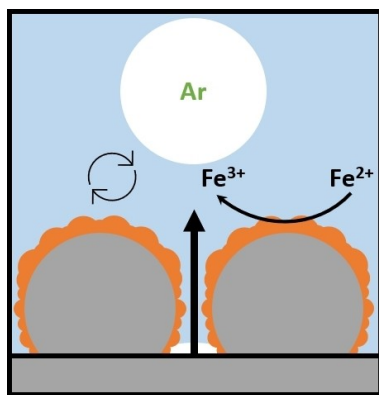
Figure 5. A) Current as a function of potential in the Fe^{II} oxidation to Fe^{III}, using 10 mM $K_4Fe(CN)_6$ in 0.5 M KCl. The dependency of the limiting current on Ar flow rate is clearly visible in the voltage range of 1.1 to 1.4 V. B) Current at 1.2 V vs RHE, from (A), as a function of Ar flow rate (Flow$_{CV}$).

ChemElectroChem

Articles
doi.org/10.1002/celc.202101135

**Chemistry
Europe**
European Chemical
Societies Publishing

Figure 6. Schematic representation of the $[Fe(CN)_6]^{4-}$ to $[Fe(CN)_6]^{3-}$ electrochemical oxidation reaction on the platinized (Orange) Ti-HFE (Grey) and the relevant mass transfer (Indicated by the arrows) at an active pore.

desorption (Heyrovsky) in which a second proton and electron are transferred [Eq. (9)] .[16,20,21]

$$H_3O^+ + e^- \rightarrow H_{ads} + H_2O \tag{7}$$

$$2H_{ads} \rightarrow H_2 \tag{8}$$

$$H_3O^+ + H_{ads} + e^- \rightarrow H_2 + H_2O \tag{9}$$

In Figure 7 the cyclic voltammetry of the HER is shown for a platinized Ti-HFE, varying the Ar flow rate in a range from 0 to 40 mL·min^{-1}. In Figure 7A multiple changes with increasing flow rate can be seen in the H_2 evolution region. In the experiment performed without any gas flow, H_2 evolution starts at a negative potential of ≈ -0.02 V, and some of the (surface adsorbed) H_2 is reversibly oxidized once the scan direction is reversed, explaining the peak at approximately ≈ -0.03 V (compare Figure S2). However, when a flow is applied through the electrode wall, these two specific features are affected. First, the onset potential for reduction shifts to slightly positive potentials (≈ 0.01 V). Second the peak of oxidation of H_2 has disappeared. In Figure 7B the reductive current is plotted against flow rate (at -30 mV), at first sight showing a less linear trend than observed for the oxidation of Fe(II). However, when the trend above approximately 15 mL·min^{-1} gas flow is considered, the increase in current (by approximately $37-33 = 4$ mA) is actually similar to observed in Figure 5B (by approximately $9-5 = 4$ mA). The initially very large increase in current is likely related to forced removal of H_2 gas from the surface by the exiting inert gas, while the second phase of the curve is related to i) the increasing participation of smaller pores of the fibre, and ii) convective mixing, enhancing proton transport towards the surface. Both phenomena are illustrated in Figure 8.
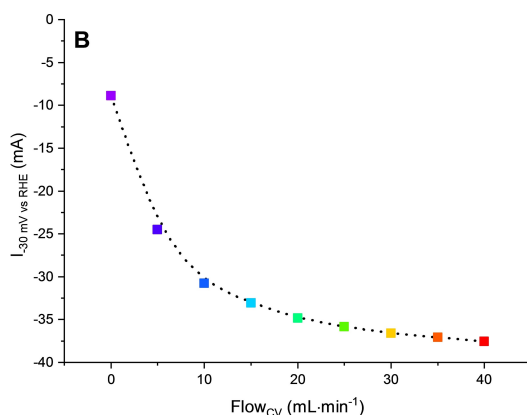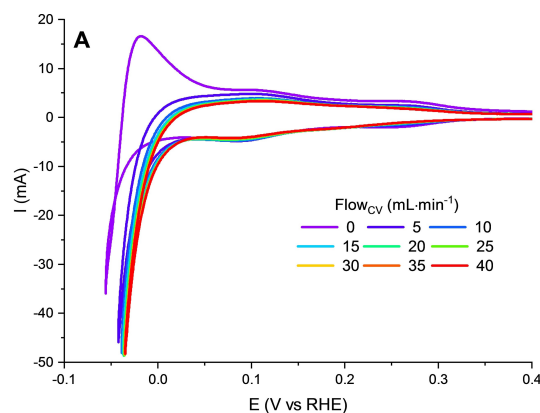

Figure 7. A) The I–V curves of hydrogen evolution on a platinized titanium hollow fibre electrode (50 mV·s^{-1}) recorded at several Ar flow rates, in 1.0 M HClO$_4$. B) The current at -30 mV vs RHE as a function of Ar flow rate through the electrode wall.
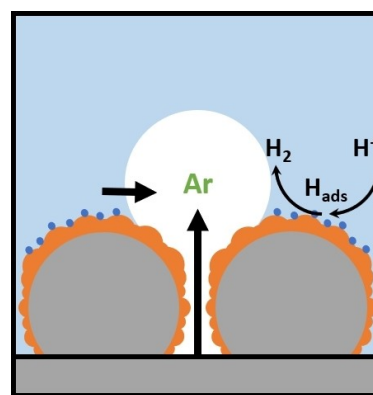

Figure 8. Schematic representation of the hydrogen evolution reaction (HER) on the platinized (Orange) Ti-HFE (Grey) and the relevant mass transfer phenomena (Indicated by the arrows) at a pore, with the small blue circles representing H_2 bubbles.

The mass transfer coefficient at high exiting flow rates

We will now roughly estimate the mass transfer coefficient as a function of gas flow in the relatively high range from 15 to 40 mL·min^{-1} for the oxidation of Fe(II) and the hydrogen evolution. The value can be calculated by Equation (10), in

ChemElectroChem

Articles
doi.org/10.1002/celc.202101135

**Chemistry
Europe**

European Chemical
Societies Publishing

which K_M is the mass transfer coefficient, I_L the limiting current, n the number of electrons transferred in the reaction, F the Faraday constant, A the electrochemical surface area (ECSA) and C the concentration of the reactant. For the ECSA we used a value of 35 cm^2.

$$K_M = \frac{I_L}{nFAC} \qquad (10)$$

A linear relation between the flow rate and K_M is shown in Figure 9 for the oxidation of Fe(II), and only in the range of high flow rates for the formation of H$_2$. The values of K_M for the oxidation of Fe(II) are not unlike the order of magnitude reported for rotating disk electrodes at rotation velocities of a few thousands rpm. This suggests that the Nernst diffusion layer obtained by the gas exiting a pore in HFEs is similar to obtained by rotation in rotating disk electrodes, but certainly this requires further systematic investigation. The K_M values for the hydrogen evolution reaction are two orders of magnitude smaller than for the oxidation of Fe(II), and thus significantly smaller than typically obtained for RDEs. We speculate this is related to the gas evolution, effecting the fractional surface area in contact with the electrolyte, but, again, this requires further investigation.
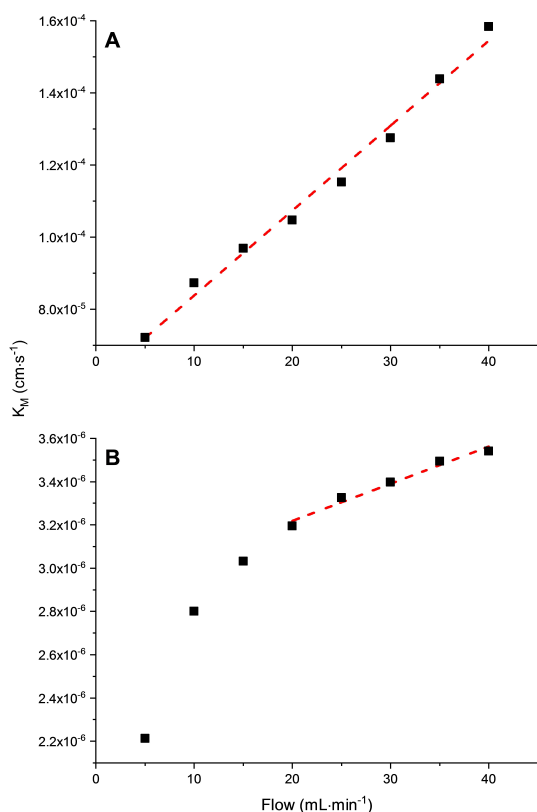
Conclusion

We have demonstrated that the morphology, and degree of decoration of Pt obtained by electrodeposition on Ti particles present near the wall of a HFE, is strongly dependent on the value of the inert gas flow that is applied during deposition. We explain these differences by i) the degree to which the relatively smaller pores are participating in the exiting gas flow, and ii) by the enhanced convective mixing near the fibre wall induced by exiting gas. Further insight in the enhancement of electrochemical currents by exiting flow was obtained by analysis of the oxidation of Fe(II) to Fe(III), and the hydrogen evolution reaction, using the platinized HFEs. For the oxidation of Fe(II) to Fe(III), at gas flow rates > 5 mL·min^{-1}, a linear relation between gas flow rate and the mass transport coefficient (K_M) is obtained, of which the values are in the same order of magnitude as obtained for electrochemistry using Rotating Disk electrodes. The values for K_M in the hydrogen evolution are smaller, likely due to additional phenomena, such as the required removal of H$_2$ gas from the surface and pores of the HFEs. The insights obtained in this work allow for a better interpretation of the literature available on HFEs, and show further investigation of mass transport phenomena is required to optimize utilization of HFEs in electrochemical processes.

Experimental Section

Materials

Dry-wet spinning

Titanium powder (ASTM, grade 2), with a particle size average of 6 μm, was obtained from TLS Technick GmbH & Co. Polyethersulfone (PES, Ultrason E 6020P, BASF) was used as binder, and N-methylpyrrolidone (NMP, Sigma-Aldrich) as solvent.

Electrochemical experiments

Silver epoxy (CW2400, CHEMTRONICS) and two-component adhesive (10550024, WEICON) were used to assemble the Hollow Fibre electrode, and include this in an electrochemical cell. H$_2$PtCl$_6$ ($\geq$ 99.9% trace metals basis, Sigma-Aldrich), HCl (ACS reagent, 37%, Sigma-Aldrich), HClO$_4$ (ACS reagent, 70%, Sigma-Aldrich), K$_4$Fe-(CN)$_6$·3H$_2$O (BioUltra, $\geq$ 99.5% (RT), Sigma-Aldrich), K$_3$Fe(CN)$_6$ (BioUltra, $\geq$ 99.0% (RT), Sigma-Aldrich), KCl (EMSURE $\geq$ 99.5%, Merck) and MilliQ water (18.2 MΩ·cm, $\leq$ 5 ppb) were used as received in the electrochemical experiments.

Methods

Dry-wet spinning

The titanium hollow fibre electrodes were produced by the previously published dry-wet spinning method and subsequent thermal treatments.[5] During dry-wet spinning the spinning mixture (Ti powder, PES binder and NMP solvent) is introduced to a non-solvent, in this case water. Solvent exchange occurs between the solvent and non-solvent resulting in a phase inversion of the polymer, or in other words solidification of the previously dissolved

Figure 9. Mass transfer coefficients (K_M) in relation to the Ar flow rate through the Pt@Ti-HFE for the oxidation of Fe(II) and the hydrogen evolution reaction. The dashed red line indicates the range of flow rates in which a linear increase in current is observed.

ChemElectroChem

Articles
doi.org/10.1002/celc.202101135

**Chemistry
Europe**

European Chemical
Societies Publishing

binder. The polymer is removed from the inorganic/polymer matrix by thermal decomposition and a porous inorganic structure, the hollow fibre electrode, remains. The characterization and properties of the Ti-HFEs are reported in a separate study.[5]

Electrochemical experiments

Assembly

The titanium hollow fibre electrodes (HFE) were assembled by potting the titanium hollow fibre (3.5 cm) in a stainless steel tube (6 mm ID) with silver epoxy. The exposed silver and stainless steel were covered with a non-conductive two-component adhesive in order to accomplish a gas tight seal and prevent the conductive parts from participating in the electrochemistry. The stainless steel tube was furthermore protected by a PEEK casing. At the top of the tube a Swagelok connection allowed the connection to a gas supply. The bottom of the titanium hollow fibre was closed with the same epoxy resin. After assembly of the electrode (≈ 2.5 cm of titanium hollow fibre is exposed) gas can be purged through the wall. A photograph of this electrode assembly can be found in the supporting information, see Figure S1.

Electrochemical cell

Electrochemical experiments were performed by positioning the HFE in the centre of a cylindrical glass vessel (42 mm high, 32 mm ID). A concentric platinized titanium mesh was used as a counter electrode and placed around the edge of the vessel. The reference electrode (REF: Ag/AgCl, 3 M NaCl) was attached to the HFE assembly, which was placed in the centre of the vessel. A schematic representation of the cell is provided in Figure 10. The Nernst equation was used to convert the potential vs REF to the RHE scale.
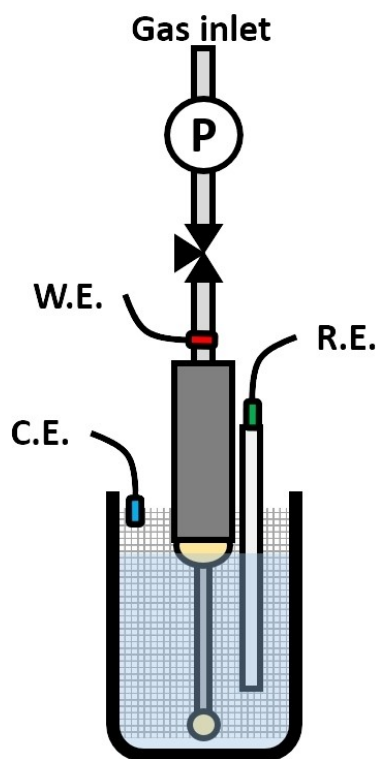

Figure 10. Schematic representation of the HFE assembly in the electro-chemical cell.

A Biologic potentiostat was used to control the potentials at the electrodes in the cell.

Electrodeposition

The electrodeposition of platinum was carried out at -0.5 V vs REF for the duration of 20 minutes. The deposition bath contained 5 mM of H_2PtCl_6 in 1 M HCl. The Ar flow rate through the electrode varied per sample, ranging from 0 to 40 mL·min^{-1} in steps of 5 mL·min^{-1}. Prior to deposition, the system was held at open circuit potential for 5 minutes, to allow the pressure on the electrode to stabilize.

Platinum electrochemical surface area

The Pt_{ECCA} was determined by the charge required for oxidation of Pt-H_{ads} (see Supplementary Information for the electrochemical data). In this experiment a 0.1 M $HClO_4$ solution was used as the electrolyte. Prior to the measurements, the Pt/Ti electrode was cycled from 0 to 1.6 V vs RHE, at 200 mV/s for a total of 100 cycles. This was done to roughen and clean the electrode. For each of the platinized samples, cyclic voltammograms were taken in the range of 0.05 to 1.5 V vs RHE, at a scan rate of 50 mV·s^{-1}. The iR-drop, as determined by the current interrupt method, was corrected for by 85 % in the potentiostat software. The positive current range obtained by scanning from 0.05 to 0.46 V vs RHE, was used to determine the Pt-H_{ads} oxidation charge. An imposed capacitive contribution, determined from the double layer region, was subtracted from this charge.[24] This method is discussed in more detail, including an example (Figure S2), in the supporting information. To arrive at a comparable number, the standard value of 210 μC·cm^{-2} was used to relate the charge to the platinum specific electrochemically active surface area .[25] These measurements were performed for every sample at all flow rates from 0 to 40 mL·min^{-1} with 5 mL·min^{-1} intervals.

Oxidation of $Fe^{II}(CN)_6^{4-}$

The oxidation of $Fe^{II}(CN)_6^{4-}$ was evaluated using electrodes which were platinized using an Ar flow at a rate of 20 mL·min^{-1}. The electrolyte consisted of 10 mM $K_4Fe(CN)_6$ and 10 mM $K_3Fe(CN)_6$ in 0.5 M KCl. Cyclic voltammetry was performed in the range of the $[Fe(CN)_6]^{3-}/[Fe(CN)_6]^{4-}$ reduction and oxidation potentials from 0.2 to 1.6 V vs RHE, with a rate of 20 mV·s^{-1}. The flow rate in the experiments was changed from 0 to 40 mL·min^{-1} in steps of 5 mL·min^{-1}, unless stated otherwise. The data presented are of the 5th forward scan, showing the oxidative current of $Fe^{II}(CN)_6^{4-}$.

Hydrogen evolution reaction

The hydrogen evolution reaction (HER) was studied in 1.0 M $HClO_4$ by cyclic voltammetry from -0.1 to 0.6 V vs RHE, applying a scan rate of 50 mV·s^{-1}.

Characterization

Scanning electron microscopy

Two microscopes were used to obtain images of the Pt-functionalized Ti HFs. A JSM-6010LA, JEOL system, was used to obtain a first indication of the Pt distribution, while a MERLIN system from ZEISS was used to obtain High Resolution images (HR-SEM).

ChemElectroChem

Articles
doi.org/10.1002/celc.202101135

Chemistry
Europe
European Chemical
Societies Publishing

X-ray photoelectron spectroscopy

The deposited platinum was analysed by X-ray photoelectron spectroscopy (XPS) using a Quantera SXM (scanning XPS microprobe) spectrometer from Physical Electronics. X-rays were generated from an Al Ka source, emitting at 1486.6 eV. A survey scan was taken, followed by core spectra of the following elements; C, O, Cl, Ti and Pt. These core spectra are shown in the supporting information, Figure S3 to S7.

Porometry

The pore size distribution of the electrodes used was determined in previous work[5] and utilized to explain the results in this manuscript. The pore size distribution was measured by capillary flow porometry, based on the liquid extrusion technique, using a Porolux 500 Porometer, high purity nitrogen and FC-43 (Perfluorotributylamine (PFTBA)) as the wetting liquid.

Acknowledgements

Conflict of Interest

The authors declare no conflict of interest.

[1] M. W. J. Luiten-Olieman, L. Winnubst, A. Nijmeijer, M. Wessling, N. E. Benes, *J. Membr. Sci.* **2011**, *370*, 124–130.

[2] M. W. J. Luiten-Olieman, M. J. T. Raaijmakers, L. Winnubst, T. C. Bor, M. Wessling, A. Nijmeijer, N. E. Benes, *J. Membr. Sci.* **2012**, *407–408*, 155–163.

[3] R. Kas, K. K. Hummadi, R. Kortlever, P. de Wit, A. Milbrat, M. W. J. Luiten-Olieman, N. E. Benes, M. T. M. Koper, G. Mul, *Nat. Commun.* **2016**, *7*, 10748.

[4] O. David, Y. Gendel, M. Wessling, *J. Membr. Sci.* **2014**, *461*, 139–145.

[5] R. P. H. Jong, P. M. Krzywda, N. E. Benes, G. Mul, *RSC Adv.* **2020**, *10*, 31901–31908.

[6] I. Merino-Garcia, J. Albo, P. Krzywda, G. Mul, A. Irabien, *Catal. Today* **2020**, *346*, 34–39.

[7] D. Bell, D. Rall, M. Großeheide, L. Marx, L. Hülsdünker, M. Wessling, *Electrochem. Commun.* **2020**, *111*, 106645.

[8] D. Liu, Y. Hu, E. Shoko, H. Yu, T. T. Isimjan, X. Yang, *Electrochim. Acta* **2021**, *365*, 137343.

[9] H. Rabiee, L. Ge, X. Zhang, S. Hu, M. Li, S. Smart, Z. Zhu, Z. Yuan, *Appl. Catal. B* **2021**, *286*, 119945.

[10] W. G. Anderson, *J. Pet. Technol.* **1987**, *39*, 1283–1300.

[11] S. Bannwarth, H. Breisig, V. Houben, C. Oberschelp, M. Wessling, *J. Membr. Sci.* **2017**, *542*, 352–366.

[12] F. Rupp, R. A. Gittens, L. Scheideler, A. Marmur, B. D. Boyan, Z. Schwartz, J. Geis-Gerstorfer, *Acta Biomater.* **2014**, *10*, 2894–2906.

[13] K. W. Peter, J. P. Robert, *J. Colloid Interface Sci.* **1996**, *184*, 550–563.

[14] P. Boissonneau, P. Byrne, *J. Appl. Electrochem.* **2000**, *30*, 767–775.

[15] C. Gabrielli, F. Huet, R. P. Nogueira, *Electrochim. Acta* **2005**, *50*, 3726–3736.

[16] V. S. Bagotsky, *Fundamentals of Electrochemistry*, John Wiley & Sons, Inc., Hoboken, New Jersey, **2006**.

[17] L. M. Torres, A. F. Gil, L. Galicia, I. González, *J. Chem. Educ.* **1996**, *73*, 808–810.

[18] S. Tanimoto, A. Ichimura, *J. Chem. Educ.* **2013**, *90*, 778–781.

[19] A. J. Bard, L. R. Faulkner, *Electrochemical Methods: Fundamentals and Applications*, John Wiley & Sons, Inc., New York, **2001**.

[20] T. Shinagawa, A. T. Garcia-Esparza, K. Takanabe, *Sci. Rep.* **2015**, *5*, 13801.

[21] N. Dubouis, A. Grimaud, *Chem. Sci.* **2019**, *10*, 9165–9181.

[22] J. Dukovic, C. W. Tobias, *Proc. Electrochem. Soc.* **1986**, *86–12*, 122–147.

[23] N. Pande, G. Mul, D. Lohse, B. Mei, *J. Electrochem. Soc.* **2019**, *166*, E280–E285.

[24] M. J. Boyd, A. A. Latimer, C. F. Dickens, A. C. Nielander, C. Hahn, J. K. Nørskov, D. C. Higgins, T. F. Jaramillo, *ACS Catal.* **2019**, *9*, 7578–7587.

[25] M. Lukaszewski, M. Soszko, A. Czerwiński, *Int. J. Electrochem. Sci.* **2016**, *11*, 4442–4469.